Chinese Chemical Letters 35 (2024) 109235

Contents lists available at ScienceDirect

Chinese Chemical Letters

journal homepage: www.elsevier.com/locate/cclet

# Two UV organic-inorganic hybrid antimony-based materials with superior optical performance derived from cation-anion synergetic interactions

Pu Zhang[a], Xiang Mao[a], Xuehua Dong[a,*], Ling Huang[a], Liling Cao[a], Daojiang Gao[a], Guohong Zou[b,*]

[a] College of Chemistry and Materials Science, Sichuan Normal University, Chengdu 610066, China
[b] College of Chemistry, Sichuan University, Chengdu 610065, China

ARTICLE INFO

*Article history:*
Received 7 September 2023
Revised 2 October 2023
Accepted 23 October 2023
Available online 26 October 2023

*Keywords:*
Antimony-based crystals
Cation-anion synergetic interactions
Large birefringence
Short UV absorption edge
Organic-inorganic hybrid
Ionothermal synthesis

ABSTRACT

Finding suitable strategies to effectively enhance the optical properties of materials are the goal being pursued by researchers. Herein, cation-anion synergetic interactions strategy was proposed to develop two novel organic-inorganic hybrid antimony-based optical materials, $(C_3H_5N_2)SbF_2SO_4$ (**I**) and $(C_5H_6N)SbF_2SO_4$ (**II**), which were obtained by introducing $Sb^{3+}$cation containing stereochemically active lone-pair (SCALP) and organic $\pi$-conjugated cations into sulphate system. The synergistic interactions of the organic $\pi$-conjugated cations, the inorganic $[SbO_2F_2]^{3-}$ seesaw anions and the $[SO_4]^{2-}$ distorted tetrahedra anions make their ultraviolet (UV) absorption edges approach 297 and 283 nm, respectively, and raise their birefringence up to 0.193@546 nm and 0.179@546 nm, respectively. Interestingly, although the two compounds have the same stoichiometric ratio and similar one-dimensional (1D) chain structure, they show opposite macroscopic symmetry, where the NCS compound (**II**) exhibits a large second-harmonic generation (SHG) response (1.6 times that of $KH_2PO_4$). The two reported compounds are found to be promising UV optical materials in the experimental tests.



Second harmonic generation (SHG) crystals and birefringence crystals, which are two key components for solid state lasers, have a wide range of applications in many scientific and technological fields, such as photolithography, advanced instruments, optical communications, and all-solid-state lasers [1–13]. A range of optical crystal materials with excellent properties are now being discovered, such as $K_3Nb_3Ge_2O_{13}$ (0.196@546 nm, 17.5 × KDP) [14], $NH_4[LiC_3H(CH_3)O_4]$ (0.06@546 nm, 4 × KDP) [15], $Sc(HSeO_3)_3$ (0.105@1064 nm, 5 × KDP) [16], $(C_3N_6H_7)(C_3N_6H_6)HgCl_3$ (0.246@1064 nm, 5 × KDP) [17], $CaYF(SeO_3)_2$ (0.138@532 nm,) [18], $Y_3F(SeO_3)_4$ (0.038@532 nm, 5.5 × KDP) [18], $RbSn_2Cl_5$ (0.168@546 nm) [19], $K_2BaGeS_5$ (0.192@1064 nm) [20], $Ba(H_2C_6N_7O_3)_2\cdot 8H_2O$ (0.24@550 nm, 12 × KDP) [21], $CsH_2C_6N_9\cdot H_2O$ (0.55@550 nm) [22], $Cd(H_2C_6N_7O_3)_2\cdot 8H_2O$ (0.6@550 nm) [23], $Cs_4Zn_5P_6S_{18}I_2$ (0.108@546 nm, 1.1 × AGS) [24]. However, with the advancement of time, the demand for excellent optical crystals is still great, and the search for excellent optical materials is still very urgent.

According to the relationship between structure and optical properties [25,26], the introduction of the following groups into the system favours compounds that exhibit large SHG effects and birefringence: (1) The $\pi$-conjugated anions [17], such as $[CO_3]^{2-}$ [27–29], $[NO_3]^-$ [30–34], $[BO_3]^{3-}$ [35,36], and $[B_3O_6]^{3-}$ [37]; (2) The stereochemically active lone pair (SCALP) metal cations, *e.g.*, $Sb^{3+}$ [38], $Sn^{2+}$ [39,40] and $Bi^{3+}$ [41]. It is noted that $Sb^{3+}$ cation exhibits abundant geometric methods of irregular coordination, such as $[SbO_3]/[SbF_3]$ trigonal pyramids [34,42], $[SbO_4]/[SbO_2F_2]$ seesaws [43,44], $[SbO_2F_3]/[SbO_3F_3]$ polyhedral [2], which favours compounds exhibiting rich structures. While due to $Sb^{3+}$ is easy to hydrolyse, it can be challenging to study. But the hydrolysis problem was overcome by our group *via* introducing the deep eutectic solvents such as choline and urea into the system. Subsequently, a series of pure inorganic antimony-based optical crystal materials with excellent optical properties were successively synthesized, such as $CsSbF_2SO_4$ (3.0 × KDP, 0.112@1064 nm) [6], $K_2Sb(P_2O_7)F$ (4.0 × KDP, 0.157@546 nm) [45], $RbSbSO_4Cl_2$ (2.7 × KDP, 0.11@1064 nm) [46].

Similar to low eutectic solvents consisting of choline chloride and urea, ionic liquids have a low melting point and an anhy-

* Corresponding authors.
*E-mail addresses:* dongxh027@sina.com (X. Dong), zough@scu.edu.cn (G. Zou).

https://doi.org/10.1016/j.cclet.2023.109235
1001-8417/

drous environment, which provides a relatively mild and anhydrous environment to ensure that $Sb^{3+}$ cations do not undergo hydrolysis. By looking up ionic liquids, we found that ionic liquids with organic $\pi$-conjugated rings are a good choice of solvent. Usually researchers choose alkali metals/alkaline earth metals that do not have d-d and f-f leaps in order to ensure that the cut-off edge of the compound is not red-shifted. However, this would result in the fact that the A-site cation in the ABX compound does not contribute to SHG and birefringence properties, which hinders further improvement of the properties. In contrast, if the alkali metal/alkaline earth metal can be replaced by organic cations with $\pi$-conjugation rings, the A-site cation will be activated. The synergistic effect of cation-anion will lead to a significant improvement in the optical properties of the compounds. At the same time, the large size of the organic cation can make the spacing between layers or chains of the structure, which may be able to enhance the optical properties of the compounds. In addition, the designable organic ligands will make it possible to design the backbone structure and properties in a targeted manner.

Based on the research ideas mentioned above, a systematical study has been carried out on organic-inorganic hybrid antimony-based materials with organic $\pi$-conjugated ring systems. Firstly, two organic-inorganic hybrid antimony-based materials, named $(C_3H_5N_2)SbF_2SO_4$ (**I**) and $(C_5H_6N)SbF_2SO_4$ (**II**), have been successfully synthesized by introducing $Sb^{3+}$ cation containing SCALP and organic $\pi$-conjugated cations into sulphate systems. The synergistic interactions of the organic $\pi$-conjugated cations, the inorganic $[SbO_2F_2]^{3-}$ seesaw anions and the $[SO_4]^{2-}$ distorted tetrahedra anions make their UV absorption edges approach 297 nm and 283 nm, respectively, and raise their birefringence up to 0.193 and 0.179@546 nm, respectively. Interestingly, although the two compounds have the same stoichiometric ratio and similar one-dimensional (1D) chain structure, they show opposite macroscopic symmetry, with compound **I** crystallizes in the centrosymmetric (CS) space group of $P\bar{1}$ and compound **II** crystallizes in the polar noncentrosymmetric (NCS) space group of $Pca2_1$. And the NCS compound **II** exhibits a large second-harmonic generation (SHG) response (1.6 × KDP). The both of compounds are auspicious near UV optical crystals proved by experimental tests.

Synthesis: Analytical grade $[C_3H_5N_2][HSO_4]$ (Lanzhou, GreenChem ILs, 99%), $[C_5H_6N][HSO_4]$ ((Lanzhou, GreenChem ILs, 99%), $SbF_3$ (Aladdin, 99%) were used as reaction reagents without further purification. Herein, the ionothermal synthesis method, which ensure the $Sb^{3+}$ cations do not undergo hydrolysis, is used, which provides a very useful option for the subsequent growth of easily hydrolysable compounds. The reagents of $SbF_3$ (0.537 g, 3 mmol) were added in $[C_3H_5N_2][HSO_4]$ (0.499 g, 3 mmol) / $[C_5H_6N][HSO_4]$ (0.532 g, 3 mmol). Stirring the mixture for 20 min, then placed the solution into a 23 mL autoclave with a Teflon liner. Heated the autoclave in an oven at 85 °C for 5 days and then cooled slowly to room temperature at a rate of 3 °C/h. After washing with acetone, colourless transparent block/rod crystals (Fig. S1 in Supporting information) were obtained in 46%–50% yield (based on Sb).

The compound **I** crystallizes in the $P\bar{1}$ (NO. 2), which is CS space group. There are one independent Sb atom, one S atom, two F atoms, one $[C_3H_5N_2]^+$ group and four O atoms in one asymmetric unit. The crystal structure of compound $(C_3H_5N_2)SbF_2SO_4$ is composed of the $[SO_4]^{2-}$ tetrahedra, the $[SbO_2F_2]^{3-}$ seesaw complex and the organic $\pi$-conjugated $[C_3H_5N_2]^+$ groups as charge balancing cations. The $[SO_4]^{2-}$ tetrahedra is formed by one S atom coordinated with four O atoms (Fig. 1a). The $[SbO_2F_2]^{3-}$ seesaw is formed by one Sb atom coordinated with two dangling F and two bridging O atoms (Fig. 1a). The $[SbF_2O_2SO_4]^{5-}$ 1D chain is formed by $[SbO_2F_2]^{3-}$ anions connected with $[SO_4]^{2-}$ anions *via* bridging oxygen atoms (Fig. 1b). The organic $\pi$-conjugated $[C_3H_5N_2]^+$ cations (Fig. 1c) are located between chains, and the 1D-helical chains are connected to each other to the three dimensional (3D) framework *via* N–H···O and N–H···F hydrogen bonds (Fig. 1d).

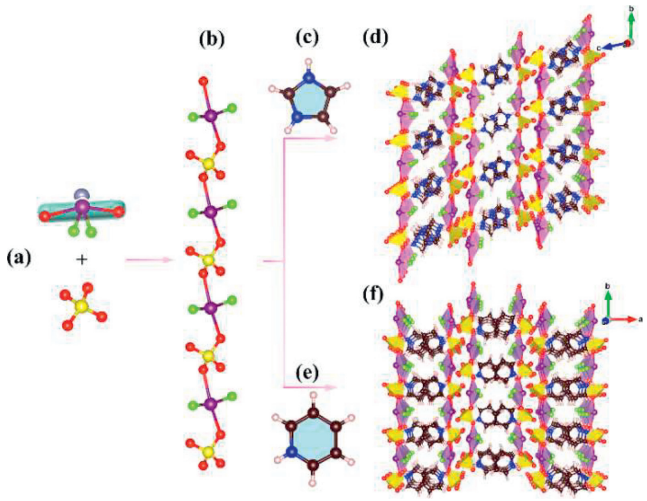


**Fig. 1.** (a) The $[SbO_2F_2]$ and $[SO_4]$ groups. (b) A 1D helical chain of $[SbF_2O_2SO_4]^{5-}$. (c) The $\pi$-conjugated protonated imidazole cation. (d) The 3D framework of compound **I** viewed along the *a*-axis. (e) The $\pi$-conjugated protonated pyridine cation. (f) The 3D framework of compound **II** viewed along the *c*-axis. Sb purple, S yellow, C black, O red, N blue, F green, H white.

The compound **II** crystallizes in the NCS space group of $Pca2_1$ (No. 29). There are one independent Sb atom, one S atom, two F atoms, one $[C_5H_6N]^+$ (Fig. 1e) group and four O atoms in an asymmetric unit. The compound **II** has a similar structure to compound **I**, the same $[SO_4]^{2-}$ tetrahedral and $[SbO_2F_2]^{3-}$ seesaw are present. Except that in compound structure **II**, it is the organic $\pi$-conjugated $[C_5H_6N]^+$ cations that acts as the charge-balancing cations between chains. The 1D-helical chains are in contact with each other to the 3D framework *via* N–H···O and N–H···F hydrogen bonds (Fig. 1f). And the bond length information of two title compounds for the moiety is shown in Fig. S2 (Supporting information).

The experimental powder X-ray diffraction (XRD) patterns of the compounds **I** and **II** are consistent with the calculated patterns fitted from the single-crystal XRD data analysis (Fig. S3 in Supporting information), confirming that the samples are phase pure.

Fig. S4 (Supporting information) shows the results of the thermogravimetric analysis. Compounds **I** and **II** were stable up to 250 and 200 °C, respectively. And the decomposition products of two compound both were confirmed to be $SbO_2$, which is demonstrated that PXRD patterns (Fig. S5 in Supporting information).

Fig. S6 (Supporting information) shows the infrared (IR) spectra of two title compounds. The moderate absorption bands viewed at 1133, 1040 $cm^{-1}$ for compound **I** and strong absorption bands viewed at 1184, 989 $cm^{-1}$ for compound **II** can be allocated to $\upsilon_3$ $SO_4$ asymmetric stretching. The absorption peaks at 938, 896 $cm^{-1}$ and 934 $cm^{-1}$ in two compounds are the result of the stretching vibration of $\upsilon_1$ $SO_4$ which is symmetric, respectively. The characteristic absorption peaks found at 620, 532 $cm^{-1}$ for compound **I** can be allocated to Sb-O/F asymmetric stretching and the bending of Sb-O/F bonds, respectively. Similarly, the Sb-O/F asymmetric stretching and the bending of Sb-O/F bonds for compound **II** can be viewed at 625, 535 $cm^{-1}$, respectively. The bands viewed at 3163/1587 $cm^{-1}$ and 3083, 1544 $cm^{-1}$ belong to the stretching vibration of N–H and the bending vibration of N–H, respectively. The peaks at 1184, 752 $cm^{-1}$ of compound **I** can be assigned to the stretching vibration and asymmetric stretching vibration of imidazole ring, respectively, and the bands at 1493, 748 $cm^{-1}$ of com-

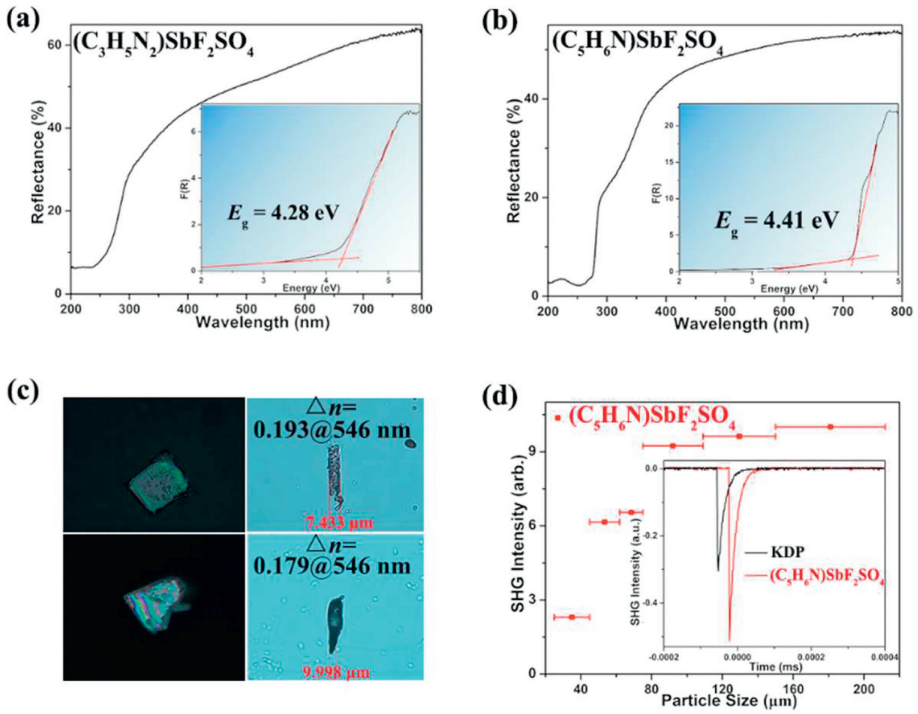


**Fig. 2.** (a, b) The UV–vis diffuse reflection spectra for **I** and **II** powder. (c) Experimental birefringence of **I** and **II** crystals. (d) The powder SHG measurement of compound **II**. The insets show the SHG intensity for the compound **II** and KDP samples.

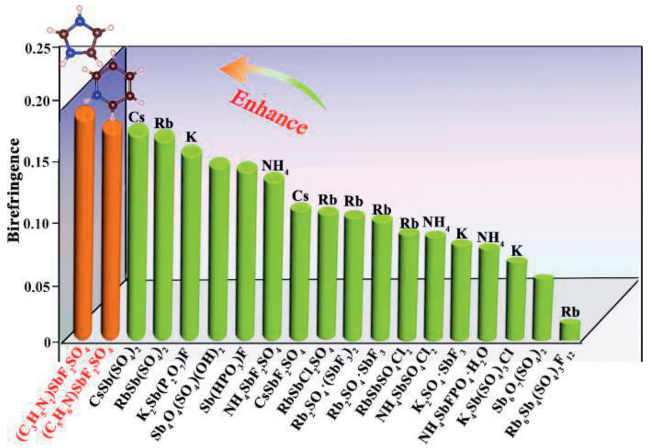


**Fig. 3.** Comparisons of the birefringence of the reported compounds and most other antimony-based optical crystals containing tetrahedra anions.

pound **II** belong to the vibration of pyridinium cation. The above characteristic absorption peak findings are in agreement with the compounds reported so far [6,43,47].

Figs. 2a and b show the UV–vis diffuse reflectance spectra of two title compounds. The optical band gap of two compounds are 4.17 and 4.38 eV, respectively, with the UV cutoff edges of 297 and 283 nm, respectively, which is an indication that they may be optical crystals in the short-wave UV range.

A ZEISS Axio A5 polarising microscope was used to measure the birefringence of two title compounds (Fig. 2c). The measurements of birefringence are 0.193@546 nm and 0.179@546 nm for **I** and **II** crystals, respectively. As shown in Fig. 3, when the $\pi$-conjugated organic cations are used to replace conventional alkali and alkaline earth metals, the cations are activated. Due to the synergistic effect of $\pi$-conjugated organic cations, $Sb^{3+}$-based polyhedra and $[SO_4]^{2-}$ anionic tetrahedra, compared to most other antimony based optical crystals containing tetrahedral anions, the birefringence of the titled compounds are significantly higher., *e.g.*, $CsSb(SO_4)_2$ (0.174@546 nm) [43], $RbSb(SO_4)_2$ (0.171@546 nm) [43], $K_2Sb(P_2O_7)F$ (0.157@546 nm) [45], $Sb(HPO_3)F$ (0.149@546 nm) [48], $Sb_4O_4(SO_4)(OH)_{21}$ (0.147@1064 nm) [42], $NH_4SbF_2SO_4$ (0.138@1064 nm) [49], $CsSbF_2SO_4$ (0.112@1064 nm) [6], $RbSbCl_2SO_4$ (0.11@1064 nm) [46], $Rb_2SO_4{\cdot}(SbF_3)_2$ (0.11@1064 nm) [50], $RbSbF_2SO_4$ (0.1@1064 nm) [44], $Rb_2SO_4{\cdot}SbF_3$ (0.09@1064 nm) [51], $NH_4SbSO_4Cl_2$ (0.09@1064 nm) [52], $K_2SO_4{\cdot}SbF_3$ (0.08@1064 nm) [51], $NH_4SbFPO_4{\cdot}H_2O$ (0.08@1064 nm) [53], $K_4Sb(SO_4)_3Cl$ (0.066@546 nm) [54], $Sb_6O_7(SO_4)_2$ (0.052@546 nm) [55], $Rb_6Sb_4(SO_4)_3F_{12}$ (0.01@1064 nm) [56].

To further illustrate the contribution of functional groups to the birefringence in the compounds above, the detailed analysis of the micromechanics is carried out. Because birefringence in crystals arises from the efficient overlapping of the microscopic polarisation anisotropies of all birefringently active groups, that are reflected in their spatial orientation and density. Herein, we have obtained from theoretical calculations that two compounds both are biaxial crystals ($n_z > n_y > n_x$). This means that the greater the number of birefringent functional groups acting on the optical principal axis Z is, the larger birefringence it obtains. So, to investigate their contribution to birefringence, the relationship between the YZ plane (bc plane for I, ab plane for II) and the orientation of the lone pair electrons in $Sb^{3+}$ cations and the $\pi$-conjugated organic cations planes is therefore important. The smaller the angle between the direction of lone pairs and the YZ plane is, the larger the contribution of the metal cations with SCALP to birefringence will be. As shown in Figs. 4a and c, the angles between the lone pair electron of $Sb^{3+}$ and YZ plane are 9.414° and 7.917°, separately. And the dihedral angles between the $\pi$-conjugated organic cations and YZ plane are 7.834° and 16.105°, separately (Figs. 4b and d). These results show that the organic $\pi$-conjugated cations ($[C_3H_5N_2]^+$ and $[C_5H_6N]^+$), the inorganic $[SbO_2F_2]^{3-}$ seesaw anions contribute significantly to the optical properties of both examples of compounds. As shown in Table S6 (Supporting information), we calculated the contribution of $[SbO_2F_2]^{3-}$ anions, $[C_3H_5N_2]^+$ and $[C_5H_6N]^+$ cations to birefringence in a unit cell. The results

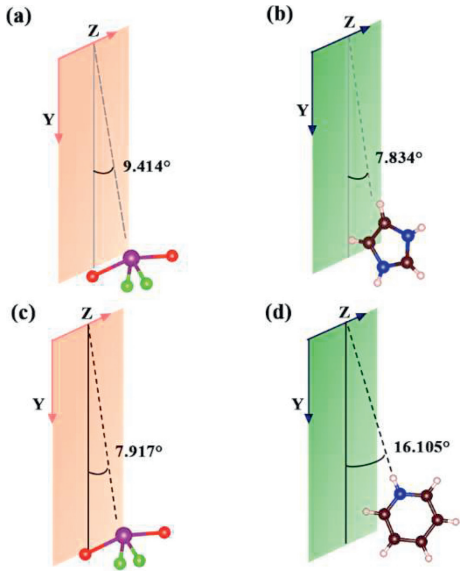


**Fig. 4.** (a, c) The angles between the lone pair electron of $Sb^{3+}$ and YZ plane of (a) compound **I**, (c) compound **II**. The dihedral angles of the $\pi$-conjugated organic cations and YZ plane of (b) compound **I**, (d) compound **II**.

also further confirm that the anionic and cationic synergistic strategy makes the compounds display large birefringence.

The 1064 nm Q-switch laser based on the Kurtz–Perry method was used for measuring the powder SHG intensities of compound **II**. As shown in Fig. 2d. The SHG intensity gradually increased as the particle sizes increase, demonstrating that the material is phase-matchable (type I) in the short-wave UV and visible light regions. And the material shows a large SHG effect that is approximately 1.6 times greater than that of KDP.

To further investigate how structure relates to optical properties, both of them were calculated based on density functional theory. The band gaps of both compounds were calculated at approximately 3.98 and 3.85 eV, respectively, indicating that the calculated values is lower than the measuring one (Fig. S7 in Supporting information).

Within Kleinman symmetry limits, compound **II** has three independent SHG tensors ($d_{15}$, $d_{24}$, and $d_{33}$). The maximum of the SHG tensor is $1.0 \times 10^{-9}$ esu@ 1064 nm (1.165 eV), which is in line with our experimental value (Fig. S8 in Supporting information). Both of the compounds belong to biaxial crystals by revealing of the refractive index dispersion curves. The calculated birefringence ($\Delta n$) is about 0.198@546 nm and 0.180@546 nm, respectively, that coincides well with the experimental one (Figs. 5a and d).

The total and partial state densities (TDOS/PDOS) are calculated for two title compounds (Figs. 5b and e), which indicate that in the range of −10 eV to 0 eV, the main components are consist of C-2p, N-2p, O-2p, F-2p, S-3p orbitals. The C-2p, N-2p, Sb-5p orbitals make significant contribution to the range of 0 eV to 10 eV. As is known to all, the optical properties of compound are major from electron transitions near the forbidden band. Obviously, the $[C_3H_5N_2]^+$ groups, $[C_5H_6N]^+$ groups, the $[SO_4]^{2-}$ distorted tetrahedral and the $[SbO_2F_2]^{3-}$ seesaws are basically responsible for the optical properties, which can also be verified by the electron-density difference (EDD) maps (Figs. 5c and f), the asymmetric electron clouds on $Sb^{3+}$ demonstrate that the lone electron pairs are stereochemically active, moreover, the electron clouds on $[C_3H_5N_2]^+$ and $[C_5H_6N]^+$ $\pi$-conjugated cations generate large optical anisotropy.

In summary, two novel organic-inorganic hybrid antimony-based optical crystals, $(C_3H_5N_2)SbF_2SO_4$ (**I**) and $(C_5H_6N)SbF_2SO_4$ (**II**), have been successfully synthesised by combining $Sb^{3+}$ cation containing SCALP and organic $\pi$-conjugated cations into the sulfate system by the ionothermal synthesis method. *Via* cation-anion synergistic strategy, the birefringence of title compounds raise up to 0.193 and 0.179@546 nm, respectively, and the UV absorption edges of them approach 297 and 283 nm, respectively, that implies both of **I** and **II** are favourable short wave UV birefringent crystals. Interestingly, although they have the same stoichiometric ratio and similar 1D chain structure, they exhibit opposite macroscopic symmetry. And the NCS compound $(C_5H_6N)SbF_2SO_4$ is type-I phase matching with the SHG efficiency about 1.6 times that of KDP. This work will provide effective research ideas and methods for high-performance UV birefringent materials and nonlinear materials in the future.

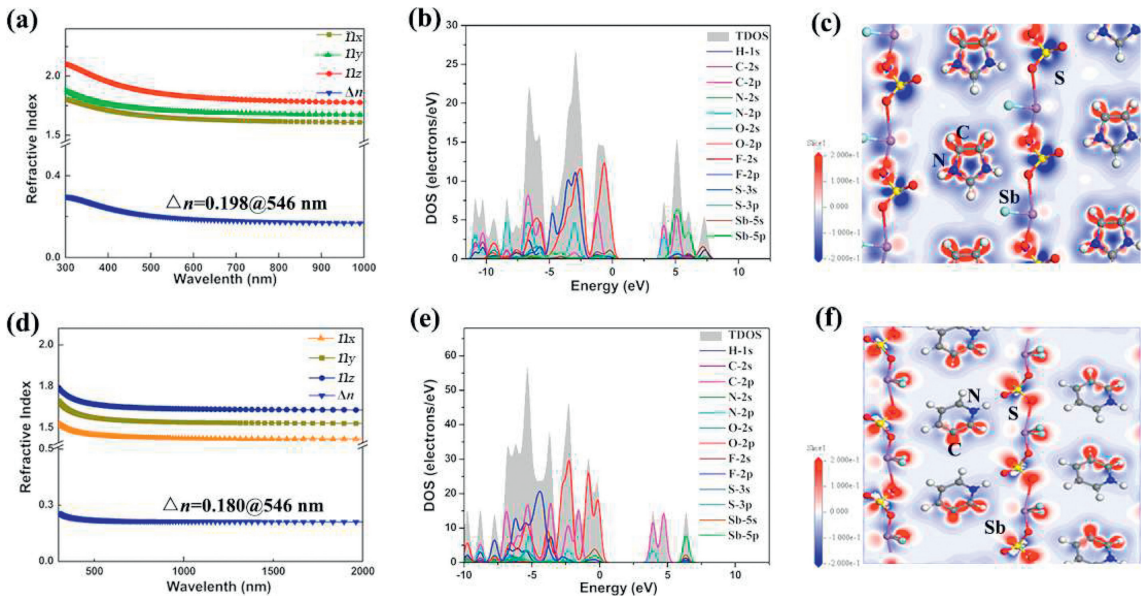


**Fig. 5.** Calculated refractive indices of compound (a) I, (d) II. Total and partial density of states of compound (b) I, (e) II. Electron density difference maps of compound (c) I, (f) II.

## Declaration of competing interest

The authors declare that they have no known competing financial interests or personal relationships that could have appeared to influence the work reported in this paper.

## Acknowledgments

The authors thank Dr. Daichuan Ma at Analytical and Testing center, Sichuan University for technical help in the Material Studio calculations. This work was supported by the National Natural Science Foundation of China (Nos. 22122106, 22071158, 21971171, 22305166), the Fundamental Research Funds from Sichuan University (No. 2021SCUNL101), the Natural Science Foundation of Sichuan Province (No. 2023NSFC1066).

## Supplementary materials

Supplementary material associated with this article can be found, in the online version, at doi:10.1016/j.cclet.2023.109235.

## References

[1] D. Cyranoski, Nature 457 (2009) 953–955.
[2] D. Zhang, Q. Wang, T. Zheng, et al., Sci. China Mater. 65 (2022) 3115–3124.
[3] G.J. Yi, G.H. Zou, Chin. J. Struct. Chem. 42 (2023) 100020.
[4] X.H. Dong, L. Huang, H.M. Zeng, et al., Angew. Chem. Int. Ed. 61 (2022) e2021167.
[5] L. Wang, F. Yang, X.Y. Zhao, et al., Dalton Trans 48 (2019) 15144–15150.
[6] X.H. Dong, L. Huang, C.F. Hu, et al., Angew. Chem. Int. Ed. 58 (2019) 6528–6534.
[7] Y. Zhou, Y.Q. Li, Q.R. Ding, et al., Chin. Chem. Lett. 32 (2021) 263–265.
[8] G.H. Zou, K.M. Ok, Chem. Sci. 11 (2020) 5404–5409.
[9] X.H. Dong, Y. Long, L. Huang, et al., J. Mater. Chem. C. 10 (2022) 17577–17582.
[10] X.H. Dong, Y. Long, L. Huang, et al., Inorg. Chem. Front. 9 (2022) 6441–6447.
[11] M. Mutailipu, J. Han, Z. Li, et al., Nat. Photon. 17 (2023) 694–701.
[12] X. Chen, Y.Q. Li, J.H. Luo, et al., Chin. J. Struct. Chem. 42 (2023) 100044.
[13] T. Ouyang, Y.G. Shen, S.G. Zhao, et al., Chin. J. Struct. Chem. 42 (2023) 100024.
[14] K.C. Chen, C.S. Lin, J.D. Chen, et al., Angew. Chem. Int. Ed. 62 (2023) e202217039.
[15] H.T. Tian, C.S. Lin, Y.Q. Zhou, et al., Angew. Chem. Int. Ed. 62 (2023) e202304858.
[16] Z. Bai, J. Lee, H. Kim, et al., Small 19 (2023) 2207709.
[17] Z. Bai, J. Lee, H. Kim, et al., Small 19 (2023) 2301756.
[18] P.F. Li, C.L. Hu, F. Kong, et al., Angew. Chem. Int. Ed. 62 (2023) e202301420.
[19] J. Guo, J. Huang, A. Tudi, et al., Angew. Chem. Int. Ed. 62 (2023) e202304238.
[20] W. Xie, F. Li, J. Chen, et al., Angew. Chem. Int. Ed. 62 (2023) e202307895.
[21] Y. Li, W. Huang, Y. Zhou, et al., Angew. Chem. Int. Ed. 62 (2023) e202215145.
[22] Y. Li, Y. Zhou, W. Huang, et al., Angew. Chem. Int. Ed. 61 (2022) e202208811.
[23] Y. Li, J. Zheng, Y. Zhou, et al., Angew. Chem. Int. Ed. 62 (2023) e202304498.
[24] X.D. Chai, M.Z. Li, S.J. Lin, et al., Small 19 (2023) 2303847.
[25] W.K. Wang, D.J. Mei, S.G. Wen, et al., Chin. Chem. Lett. 33 (2022) 2301–2315.
[26] C.C. Jin, H. Zeng, F. Zhang, et al., Chem. Mater. 34 (2022) 440–450.
[27] G.H. Zou, H. Jo, S.J. Lim, et al., Angew. Chem. Int. Ed. 57 (2018) 8619–8622.
[28] G.H. Zou, Z.E. Lin, H.M. Zeng, et al., Chem. Sci. 9 (2018) 8957–8961.
[29] Y.T. Zhang, Y. Long, X.H. Dong, et al., Chem. Commun. 55 (2019) 4538–4541.
[30] X.H. Dong, L. Huang, Q.Y. Liu, et al., Chem. Commun. 54 (2018) 5792–5795.
[31] Y. Long, X.H. Dong, H.M. Zeng, et al., Inorg. Chem. 61 (2022) 4184–4192.
[32] Y. Long, X.H. Dong, L. Huang, et al., Inorg. Chem. 59 (2020) 12578–12585.
[33] L. Wang, H.M. Wang, D. Zhang, et al., Inorg. Chem. Front. 8 (2021) 3317–3324.
[34] Q. Wang, J.X. Ren, D. Wang, et al., Inorg. Chem. Front. 10 (2023) 2107–2114.
[35] S. Zhao, P. Gong, L. Bai, et al., Nat Commun 5 (2014) 4019.
[36] J. Zhou, Y. Liu, H. Wu, et al., Angew. Chem. Int. Ed. 59 (2020) 19006–19010.
[37] W.J. Xie, Z. Feng, J.G. Mao, Inorg. Chem. 45 (2022) 18260–18266.
[38] D. Zhang, Q. Wang, T. Zheng, et al., J. Alloys Compd. 896 (2021) 162921.
[39] Y.W. Ge, Q. Wang, F. Yang, et al., Inorg. Chem. 60 (2021) 8322–8330.
[40] L.Y. Ren, L.H. Cheng, X.Y. Zhou, et al., Inorg. Chem. Front. 10 (2023) 5602–5610.
[41] X.H. Dong, Z.Z. Zhang, L. Huang, et al., Inorg. Chem. Front. 9 (2022) 5572–5578.
[42] Q. Wei, K. Wang, C. He, et al., Inorg. Chem. 15 (2021) 11648–11654.
[43] Y. Lan, J.X. Ren, P. Zhang, et al., Chin. Chem. Lett. 35 (2024) 108652.
[44] F. Yang, L.J. Huang, X.Y. Zhao, et al., J. Mater. Chem. C. 7 (2019) 8131–8138.
[45] Y.L. Deng, L. Huang, X.H. Dong, et al., Angew. Chem. Int. Ed. 59 (2020) 21151–21156.
[46] F.F. He, Y.L. Deng, X.Y. Zhao, et al., J. Mater. Chem. C. 7 (2019) 5748–5754.
[47] F. Chen, Y.Y. Ren, J.N. Guo, et al., Chem. Commun. 53 (2017) 1595–1598.
[48] Y. Long, X.H. Dong, L. Huang, et al., Inorg. Chem. 43 (2022) 16997–17001.
[49] F.F. He, Y.W. Ge, X.Y. Zhao, Dalton Trans 49 (2020) 5276–5282.
[50] Q. Wang, L. Wang, X.Y. Zhao, et al., Inorg. Chem. Front. 6 (2019) 3125–3132.
[51] F.F. He, L. Wang, C.F. Hu, et al., Dalton Trans 47 (2018) 17486–17492.
[52] F.F. He, Q. Wang, C.F. Hu, et al., Cryst. Growth Des. 18 (2018) 6239–6247.
[53] F.F. He, Y.W. Ge, X.Y. Zhao, et al., Dalton Trans. 49 (2020) 5276–5282.
[54] F. Yang, L. Wang, Y. Ge, et al., J. Alloys Compd. 834 (2020) 155154.
[55] Q. Wei, C. He, K. Wang, et al., Chem. Eur. J. 27 (2021) 5880–5884.
[56] X.H. Dong, Y. Long, X.Y. Zhao, et al., Inorg. Chem. 59 (2020) 8345–8352.